Cost-Effective High-Performance Air-Filled SIW Antenna Array for the Global 5G 26-GHz and 28-GHz Bands

Igor Lima de Paula, Sam Lemey, *Member, IEEE*, Dries Bosman, Quinten Van den Brande, Olivier Caytan, *Member, IEEE*, Joris Lambrecht, Maarten Cauwe, Guy Torfs, Hendrik Rogier, *Senior Member, IEEE*

***Abstract*—A cost-effective, compact and high-performance antenna element for beamforming applications in all 5G New Radio bands in the [24.25-29.5] GHz spectrum is proposed. The novel antenna topology adopts a square patch, an edge-plated air-filled cavity, and an hourglass-shaped aperture-coupled feed to achieve a very high efficiency over a wide frequency band in a compact footprint ($0.48\lambda_0 \times 0.48\lambda_0$). Its compliance with standard PCB fabrication technology, without complex multi-layer PCB stack, ensures low-cost fabrication. The antenna feedplane offers a platform for compact integration of active electronic circuitry. Two different modular 1×4 antenna arrays were realized to demonstrate its suitability for broadband multi-antenna systems. Measurements of the fabricated antenna element and the antenna array prototypes revealed a -10-dB impedance bandwidth of 7.15 GHz (26.8%) and 8.2 GHz (30.83%), resp. The stand-alone antenna features a stable peak gain of 7.4 ± 0.6 dBi in the [24.25-29.5] GHz band and a measured total efficiency of at least 85%. The 1×4 array provides a peak gain of 10.1 ± 0.7 dBi and enables grating-lobe-free beamsteering from -50° to 50°.**

***Index Terms*—Millimeter wave antenna arrays, air-filled substrate-integrated waveguide (AFSIW), 5G wireless communication, New Radio (NR), beamforming.**

I. INTRODUCTION

THE fifth generation (5G) of mobile telecommunications [1]–[3] requires reliable, low-latency and high-data-rate radio access networks [4]. Thereto, a significant portion of the infrastructure will exploit the large bandwidths available at millimeter wave (mmWave) frequencies [5]. Multi-antenna systems will play an essential role to reliably support multiple high-data-rate links to dynamic users [4].

For millions of small-cell base stations (BSs) and end-user terminals [6], there is a stringent need for low-cost and energy-efficient [7] multi-antenna systems with adaptive beam steering that cover multiple mmWave 5G New Radio (NR) bands. In recent years, transceivers with integrated beamforming [8], [9] have been developed. Yet, their antenna array is typically implemented in expensive, complex, high-resolution, multi-layer Printed Circuit Board (PCB) technology to realize electrically thick antenna substrates providing sufficient bandwidth [8]–[10]. Moreover, the PCB substrate inevitably limits the radiation efficiency.

This letter proposes a novel, compact, cost-effective and highly efficient air-filled substrate-integrated-waveguide (AFSIW) aperture-coupled cavity-backed patch antenna that covers the n258 ([24.25-27.5) GHz), n257 ([26.5-29.5) GHz), and n261 ([27.5-28.35] GHz) 5G bands. The AFSIW technology leads to stable and highly-efficient radiation performance, ensures full compatibility with standard PCB fabrication processes and facilitates compact integration of the active front-end module. Broadband antenna performance is achieved *(i)* by exploiting the low Q-factor of the air cavity and *(ii)* by resonant hourglass-shaped-aperture coupling to a resonant square patch in the air-filled metalized cavity. While [11] achieves a large bandwidth via an aperture-coupled patch topology, and [12]–[14] further extend it by using low-permittivity substrates, they suffer from a footprint larger than $\lambda_0/2 \times \lambda_0/2$. The metalized cavity in our topology reduces the antenna footprint to $0.48\lambda_0 \times 0.48\lambda_0$ at 26.875 GHz, by capacitively loading both resonant structures, and mitigates mutual coupling [15]. Prototypes of a stand-alone antenna element and two 1×4 arrays achieve matching from 22.5 GHz to 30.7 GHz, a total efficiency of at least 85% (for one antenna element), a stable radiation pattern with a minimal boresight gain of 9.8 dBi, and a grating-lobe-free steering range from -50° to 50°.

AFSIW stacks inexpensive dual-layer PCB laminates and, by locally removing the substrate and realizing sidewalls by either edge plating [16] or rows of vias [13], [17], implements air-filled waveguides/cavities. [16], [18]–[22] propose low-cost high-performance micro- and mmWave AFSIW components, including antennas [16], [17], [23]–[25] and waveguide-fed slot arrays [26], [27]. While the latter exhibit ultra-high radiation efficiencies, they suffer from a large footprint and a narrow bandwidth, making them less suited for broadband mmWave adaptive beam steering systems [28]. Whereas in this letter, double-layer PCB laminates realize the topology, [24] and [25] exploit drilled aluminum plates to implement the air-filled cavities, while [23] adopts standard silicon process technology for the on-chip cavity. Table I compares the measured performance of the proposed antenna to the state of the art, demonstrating best-in-class performance in terms of bandwidth, radiation efficiency and compact footprint.

This work was supported in part by ERC through "ATTO: A new concept for ultrahigh capacity wireless networks" under Grant 695495.

Igor Lima de Paula, Sam Lemey, Dries Bosman, Quinten Van den Brande, Olivier Caytan, Joris Lambrecht, Guy Torfs, and Hendrik Rogier are with the IDLab, Dept. of Information Technology, Ghent University-imec, Ghent 9052, Belgium (e-mail: igor.limadepaula@ugent.be). Maarten Cauwe is with CMST, Dept. of Electronics and Information Systems, Ghent University-imec, Ghent 9052, Belgium

II. ANTENNA/ARRAY DESIGN

A. Compact Antenna Element

We propose an antenna element that operates with a total efficiency over 85% in all worldwide-planned 26 GHz and 28 GHz 5G bands for broadband mmWave multi-antenna systems with adaptive beamforming. Thereto, its reflection coefficient with respect to 50 Ω should remain below −10 dB in the entire [24.25-29.5] GHz band. A footprint smaller than $0.53\lambda_{\min} \times 0.53\lambda_{\min}$ at 29.5 GHz is pursued for grating-lobe-free beamsteering from -50° to 50°. In addition, the antenna element should exhibit a cross-polarization discrimination (XPD) larger than 20 dB over its entire frequency band [29]. Back radiation and mutual coupling should be reduced to the bare minimum to ensure good isolation from the integration platform and to guarantee blindspot-free beamsteering, resp. Finally, the antenna should be low cost and facilitate compact integration of the front-end module to minimize the length and the insertion loss of the antenna-IC interconnections.

To fulfill these requirements, a cavity-backed patch antenna topology is implemented in stacked AFSIW technology [16], as shown in Fig. 1. To increase antenna efficiency, lossy substrate material is judiciously removed [18], while the low surface roughness minimizes the conductor losses [16], [19]. As a result, the antenna consists of three inexpensive stacked dual-layer PCBs, labeled PCB_1, PCB_2 and PCB_3. The inner layer of PCB_1 contains a square radiating patch that is backed by an air-filled edge-plated cavity, milled out in PCB_2 and metalized through edge plating. This approach protects the radiating patch from environmental effects and avoids penetration of electromagnetic fields in the lossy substrate of PCB_2, yielding highly efficient operation with minimal mutual coupling in compact arrays. The antenna feed plane on PCB_3 consists of a grounded-coplanar-waveguide (GCPW) feed-line extending over an hourglass-shaped coupling aperture at PCB_3's bottom layer. A rectangular aperture on the top ground plane ensures a proper transition between both structures. Its dimensions provide proper matching while minimizing its footprint and maintaining robustness against manufacturing tolerances. GCPW-based aperture coupling yields high XPD and ensures high isolation between feed network and antenna element [30]. The hourglass aperture offers several degrees of freedom to match the antenna input impedance to a variety of loads. Therefore, the feedplane is an ideal platform for integrating a front-end module, while the antenna's highly tunable input impedance facilitates co-optimization. Although not yielding a larger bandwidth than a rectangular aperture, the hourglass aperture makes the aperture's field distribution more uniform [30], yielding maximum coupling with the smallest aperture area to minimize back radiation.

Although conventional AFSIW structures tend to be large due to their low ϵ_r, this antenna topology achieves broad-band antenna performance in a compact antenna footprint by leveraging the air cavity to strengthen the coupling between the resonant hour-glass-shaped aperture in PCB_3 and the resonant square patch on PCB_1. By carefully dimensioning both resonant structures and the air-filled cavity, two distinct resonance frequencies are obtained at neighboring frequencies. Merged, they cover the entire [24.25-29.5] GHz band. The capacitive loading by the cavity on both resonant structures miniaturizes the antenna footprint. Fig. 2 demonstrates the effect of the dimensions of the resonant patch (L_{patch}), the cavity (W_{cav}) and the length of the resonant hourglass-shaped aperture ($L_{\text{a,hg}}$) on the antenna's reflection coefficient. All plots show two resonance frequencies, of which the lowest is related to the length of the hourglass-shaped aperture and the

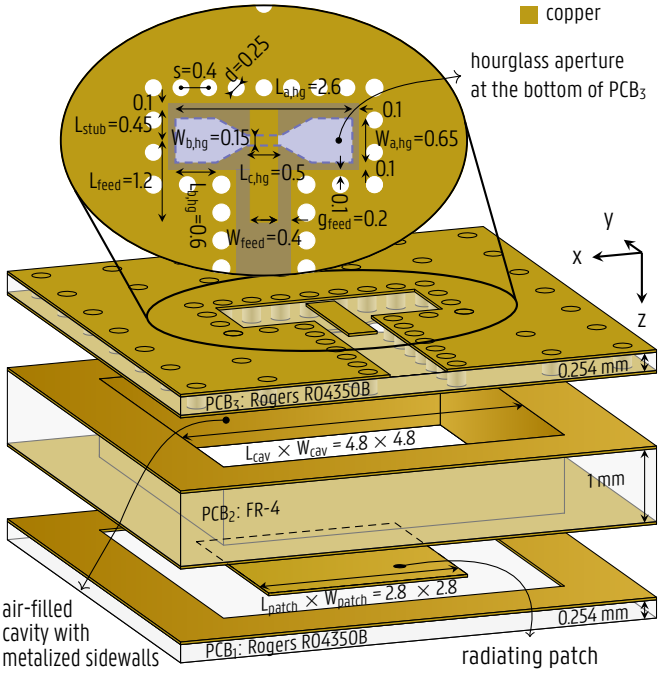

Fig. 1. AFSIW antenna with annotated dimensions (in mm). Bottom: exploded view showing the three constituent PCBs, i.e., PCB_1 (RO4350B), PCB_2 (FR4) and PCB_3 (RO4350B); inset: detail of the feedplane.

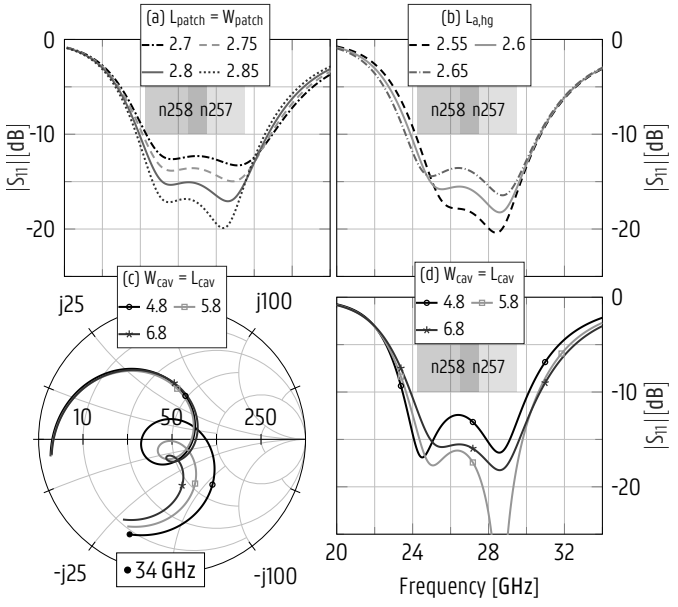

Fig. 2. Parametric analysis of the antenna element. In (a) and (b), L_{patch} and $L_{\text{a,hg}}$ are individually varied, with W_{cav} set to 6.8 mm. In (c) and (d), the optimized version, with $W_{\text{cav}} = 4.8$ mm, is compared to those with increasing cavity sizes. All parameters are expressed in mm.

highest depends on the patch size. By first fixing the cavity size to $6.8\,\mathrm{mm} \times 6.8\,\mathrm{mm}$ and increasing L_{patch}, the highest resonance frequency decreases while the lowest one remains unaltered (Fig. 2(a)). Similarly in Fig. 2(b), an increase of $L_{\mathrm{a,hg}}$ shifts the lowest resonance frequency downward, leaving the highest resonance frequency unaffected. Figs. 2 (c) and (d) show that when W_{cav} reduces from 6.8 mm to 4.8 mm, the resonance loop area increases, implying stronger coupling between patch and hour-glass aperture. Hence, the air-filled edge-plated cavity allows accurate control of the coupling mechanism, enabling antenna miniaturization and compact integration of self-shielded antenna elements.

Based on these insights, the antenna was optimized for high performance and implementation in a cost-effective and modular manner using only standard two-layer PCB laminates. All PCBs were fabricated at Eurocircuits by using standard PCB manufacturing technology [23]. A 254-µm-thick RO4350B substrate ($\tan\delta$ = 0.0037 and ϵ_{r} = 3.66) is adopted to construct PCB_1 and PCB_3 (Fig. 1). As edge plating fully eliminates the electromagnetic fields in the lossy dielectric outside the antenna cavity, PCB_2 was implemented in a cheap FR4 substrate ($\tan\delta$ = 0.024 and ϵ_{r} = 4.3) without compromising performance. A thickness of 1 mm ($0.09\lambda_0$) ensures coverage of all global 5G 26-GHz and 28-GHz bands with sufficient margin. Finally, the three PCBs are screwed together such that patch, cavity and coupling aperture are centered to each other. This approach ensures sufficient electrical contact between the stacked PCBs and yields a modular design, in which each part can be replaced later on by a different version, as shown in Section II.B. Hence, it proves a viable alternative for the approach in [18] where the stacked PCBs are soldered. The final antenna dimensions, optimized by CST Microwave Studio's frequency domain solver, are indicated in Fig. 1.

B. Antenna Array

To demonstrate our topology's 5G beamforming potential, a 1×4 antenna array was designed and manufactured. A prototype with interelement spacing 5.4 mm ($0.48\lambda_0$) is shown in Fig. 3, detailing the three PCBs composing the array. Modularity is shown by realizing two versions of the 1×4 antenna array by only replacing PCB_3. In the first version, denoted AA+WPD, $\mathrm{PCB}_{3,a}$ (Fig. 3 (a)) equally excites all antenna elements (AEs) through a two-stage Wilkinson power divider (WPD) feed network. In the second version, denoted AA, $\mathrm{PCB}_{3,b}$ (Fig. 3 (d)) independently feeds all antenna elements. Now, every other antenna feed was rotated by 180° to accommodate for mmWave connectors and measurement cables. Full-wave simulations show that this rotation does not impact the magnitude of the mutual coupling.

III. RESULTS

To measure each prototype with an *Agilent E8364B* vector network analyzer, solder-free V-type (1.85 mm) Southwest Microwave end-launch connectors were press fit onto the feedline, extended by $1.8\,\lambda_0$ to mitigate the effect of the large metallic connector. Connectors and extended feedlines were de-embedded by Thru, Reflect, Line (TRL) calibration.

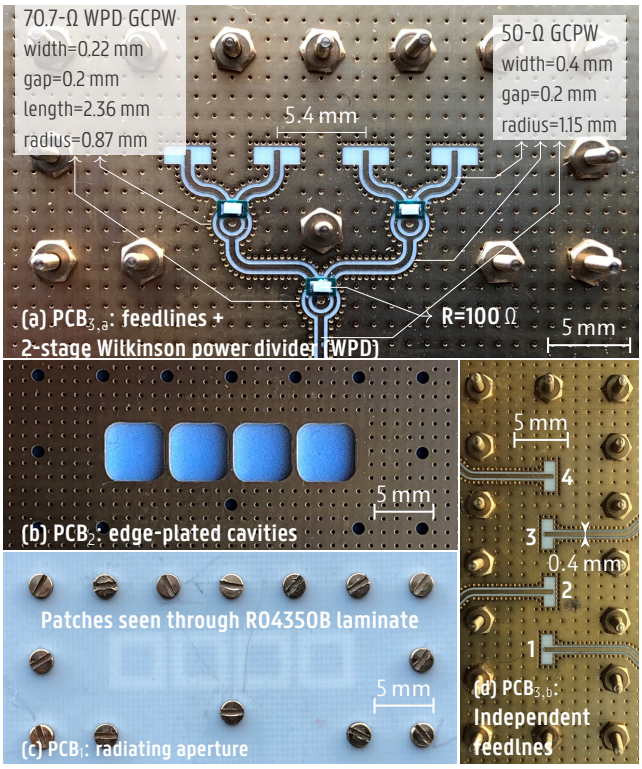

Fig. 3. PCBs composing two 1×4 antenna arrays: (a) Feedplane PCB_3 of the corporate-fed WPD-based antenna array (AA+WPD); (b) edge-plated air-filled cavities in PCB_2; (c) radiating aperture on PCB_1; (d) alternative feedplane PCB_3 with independent antenna feeds (AA).

The AE and AA+WPD achieve a measured -10-dB impedance bandwidth of 7.15 GHz (26.8 %; [23.15-30.3] GHz) and 8.2 GHz (30.83 %; [22.5-30.7] GHz), resp. Hence, both cover the [24.25-29.5] GHz band by a large margin and agree well with simulations, as seen in Fig. 4. Figure 5 shows the AA prototype's simulated (sim.) and measured (meas.) mutual coupling coefficients, achieving excellent agreement. At 24.25 GHz, where the interelement spacing is only 0.44 λ_{max}, the mutual coupling between the center elements ($|S_{23}|$) reaches −13.25 dB, while the isolation remains mostly above 15 dB otherwise and is much higher for non-adjacent elements. Similar $|S_{23}|$ curves were obtained when all screws were removed except for the corner ones, proving the effectiveness of the PCB assembly technique. Based on the meas. S-parameters of the AA, the active reflection coefficient of the center element was calculated to be below −13.1 dB, −9.8 dB and −5 dB when the beam steers to 0°, 30° and 50°, resp.

The far-field radiation patterns were measured in an anechoic chamber by an *NSI-MI* spherical antenna measurement system and a *Keysight N5242A PNA-X* VNA through gain comparison with a *WR-34* standard gain horn. A model of the V-type connector and extended feedline is included in the simulations for adequate comparison between sim. and meas. radiation patterns. Fig. 6 shows a good agreement between the sim. and meas. co-polarized radiation patterns of the AE and AA+WPD and an outstanding meas. XPD of at least 20.9 dB and 23.53 dB within their half-power beamwidth. Moreover,

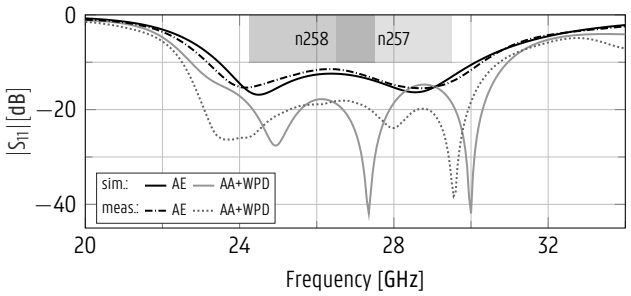

Fig. 4. Simulated (sim.) and measured (meas.) $|S_{11}|$ curves of: *(i)* antenna element (AE); and *(ii)* WPD-fed 1×4 antenna array (Array+WPD).

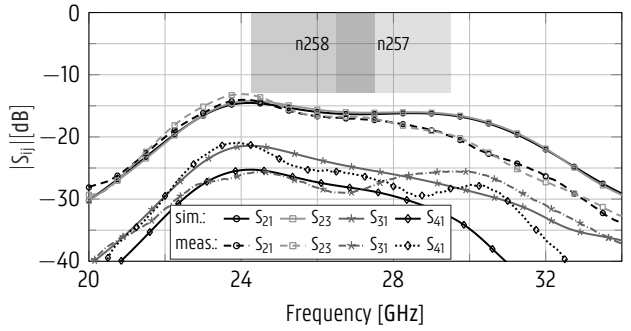

Fig. 5. Simulated and measured mutual coupling of 1×4 antenna array.

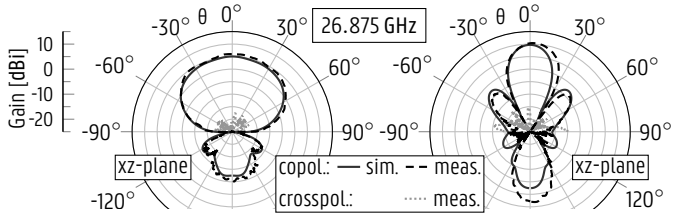

Fig. 6. Simulated and measured co- (copol.) and cross-polarized (crosspol.) radiation pattern at $f_0 = 26.875\,\text{GHz}$ of the stand-alone antenna (top) and WPD-fed 1×4 antenna array (bottom).

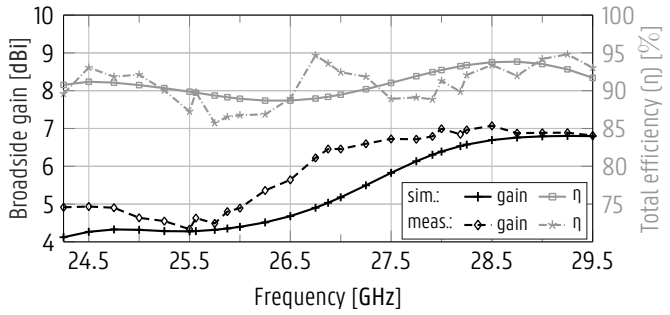

Fig. 7. AE's simulated and measured broadside gain and total efficiency.

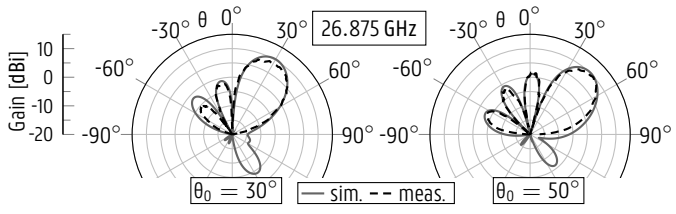

Fig. 8. Active simulated and measured radiation pattern of 1×4 antenna array at $f_0 = 26.875\,\text{GHz}$ steered to $\theta_0 = 30°$ (left) and $\theta_0 = 50°$ (right).

the broadside gain of the AE is depicted in Fig. 7. While the meas. (sim.) broadside gain varies by $\pm\,1.4\,\text{dBi}$ ($\pm\,1.3\,\text{dBi}$) in the targeted frequency band, a stable meas. (sim.) realized peak gain of $7.4 \pm 0.6\,\text{dBi}$ ($6.6 \pm 0.7\,\text{dBi}$) for the AE and $10.1 \pm 0.7\,\text{dBi}$ ($10.5 \pm 0.6\,\text{dBi}$) for the AA+WPD is obtained. As a reference, the 2-stage WPD prototype yielded an in-band insertion loss of $1.1 \pm 0.1\,\text{dB}$ per branch. The meas. and sim. embedded radiation patterns of the AA were post-processed by applying appropriate uniform-amplitude phase-shifted excitations [31] to steer the beam to 30° and 50°, as shown in Fig. 8. From -50° to 50°, the meas. realized gain is free of blindspots and lies within $9.56 \pm 0.76\,\text{dBi}$.

Fig. 7 shows the meas. total efficiency of the AE, after compensating for the additional feed line length and the connector's insertion loss. In-band antenna efficiencies larger than 85% and 80% are obtained for the AE and the AA+WPD, resp. The sim. antenna efficiency in Fig. 7 is based on a full-wave simulation without connector and extended feedline. Table I compares the meas. performance of our design to the most closely related state of the art in terms of fractional bandwidth (BW), efficiency (η) at f_0 and antenna footprint, expressed in wavelengths at f_0. The presented low-cost antenna exhibits best-in-class performance. It is excellently suited for beamforming applications in the n258, n259 and n261 bands.

TABLE I
COMPARISON OF PROPOSED SOLUTION WITH THE STATE OF THE ART.

Ref.	f_0 [GHz]	BW [%]	η [%]	at f_0	Footprint (w, l, h) $[\lambda_0^3]$
[8]	30	13	N/A		$0.5 \times 0.63 \times 0.01$
[9]	29	3	N/A		$0.54 \times 0.51 \times 0.05$
[17]	28	23	**96***		$0.63 \times 0.63 \times 0.09$
[23]	28.5	13	91		$\mathbf{0.49 \times 0.49} \times 0.05$
[13]	64.7	**36.2**	**98***		$0.67 \times 0.67 \times 0.16$
[14]	13.25	19	**98***		$0.84 \times 0.84 \times 0.07$
[11]	150	14	**96**		$\mathbf{0.44 \times 0.44} \times 0.06$
This	26.875	**26.8**	**94**		$\mathbf{0.48 \times 0.48 \times 0.09}$

* Simulated

IV. CONCLUSION

A compact, high-performance AFSIW antenna element was proposed for beamforming applications in all worldwide-planned 26 GHz and 28 GHz 5G NR bands. It leverages an edge-plated AFSIW cavity, realized in low-cost dual-layer PCB technology, to obtain a total efficiency of at least 85% over a -10-dB impedance bandwidth of 26.8% in a compact footprint ($0.48\lambda_0 \times 0.48\lambda_0$). Its suitability for active multi-antenna systems with adaptive beamsteering is guaranteed by *(i)* an isolation between adjacent antenna elements of at least 13.25 dB at an interelement spacing $< \lambda_0/2$, *(ii)* a modular approach with a feed plane tailored for compact integration of a front-end IC, and *(iii)* an antenna input impedance tunable by co-optimization. Experimental validation of two versions of a modular 1×4 antenna array revealed a stable broadside gain of $10.1 \pm 0.7\,\text{dBi}$ within the [24.25-29.5] GHz band and a beamsteering range from -50° to 50° without blindspots or grating lobes, offering a mass-manufacturable solution for 5G beamforming antenna systems.

REFERENCES

[1] ITU-R, "IMT Vision — Framework and Overall Objectives of the Future Development of IMT for 2020 and Beyond," ITU-R Rec. M.2083, Tech. Rep., 2015.

[2] J. Lee, E. Tejedor, K. Ranta-aho, H. Wang, K. Lee, E. Semaan, E. Mohyeldin, J. Song, C. Bergljung, and S. Jung, "Spectrum for 5G: Global Status, Challenges, and Enabling Technologies," *IEEE Commun. Mag.*, vol. 56, no. 3, pp. 12–18, Mar. 2018.

[3] M. Shafi, A. F. Molisch, P. J. Smith, T. Haustein, P. Zhu, P. D. Silva, F. Tufvesson, A. Benjebbour, and G. Wunder, "5G: A Tutorial Overview of Standards, Trials, Challenges, Deployment, and Practice," *IEEE J. Sel. Areas Commun.*, vol. 35, no. 6, pp. 1201–1221, Jun. 2017.

[4] M. A. Habibi, M. Nasimi, B. Han, and H. D. Schotten, "A Comprehensive Survey of RAN Architectures Toward 5G Mobile Communication System," *IEEE Access*, vol. 7, pp. 70 371–70 421, 2019.

[5] 3GPP, "Summary of Release 15 Work Items," Technical Specification Group Services and System Aspects, Tech. Rep. TR 21.915, V1.1.0, 2019.

[6] M. Maternia, S. E. E. Ayoubi, M. Fallgren, P. Spapis, Y. Qi, D. Martín-Sacristán, Óscar Carrasco, M. Fresia, M. Payaró, M. Schubert, J. S. Bedo, and V. Kulkarni, "5G PPP Use Cases and Performance Evaluation Models," 5GPPP, Tech. Rep., 2016.

[7] Y. Chen, S. Zhang, S. Xu, and G. Y. Li, "Fundamental Trade-Offs on Green Wireless Networks," *IEEE Commun. Mag.*, vol. 49, no. 6, pp. 30–37, Jun. 2011.

[8] K. Kibaroglu, M. Sayginer, T. Phelps, and G. M. Rebeiz, "A 64-Element 28-GHz Phased-Array Transceiver With 52-dBm EIRP and 8–12-Gb/s 5G Link at 300 Meters Without Any Calibration," *IEEE Trans. Microw. Theory Techn.*, vol. 66, no. 12, pp. 5796–5811, 2018.

[9] H. Kim, B. Park, S. Song, T. Moon, S. Kim, J. Kim, J. Chang, and Y. Ho, "A 28-GHz CMOS Direct Conversion Transceiver With Packaged 2×4 Antenna Array for 5G Cellular System," *IEEE J. Solid-State Circuits*, vol. 53, no. 5, pp. 1245–1259, 2018.

[10] M. Mosalanejad, S. Brebels, I. Ocket, C. Soens, G. A. E. Vandenbosch, and A. Bourdoux, "Millimeter Wave Cavity Backed Aperture Coupled Microstrip Patch Antenna," in *2016 10th European Conference on Antennas and Propagation (EuCAP)*, Apr. 2016, pp. 1–5.

[11] A. Lamminen, J. Säily, J. Ala-Laurinaho, J. de Cos, and V. Ermolov, "Patch Antenna and Antenna Array on Multilayer High-Frequency PCB for D-Band," *IEEE Open Journal of Antennas and Propagation*, vol. 1, pp. 396–403, 2020.

[12] M. Bilgic and K. Yegin, "High Gain, Wideband Aperture Coupled Microstrip Antenna Design Based on Gain-Bandwidth Product Analysis," *Applied Computational Electromagnetics Society Journal*, vol. 29, pp. 560–567, Aug. 2014.

[13] I. M. Mohamed and A. Sebak, "60 GHz 2-D Scanning Multibeam Cavity-Backed Patch Array Fed by Compact SIW Beamforming Network for 5G Applications," *IEEE Trans. Antennas Propag.*, vol. 67, no. 4, pp. 2320–2331, 2019.

[14] S. K. Pavuluri, C. H. Wang, and A. J. Sangster, "A High-Performance Aperture-Coupled Patch Antenna Supported by a Micromachined Polymer Ring," *IEEE Antennas Wireless Propag. Lett.*, vol. 7, pp. 283–286, 2008.

[15] T. Y. Yang, W. Hong, and Y. Zhang, "Wideband Millimeter-Wave Substrate Integrated Waveguide Cavity-Backed Rectangular Patch Antenna," *IEEE Antennas Wireless Propag. Lett.*, vol. 13, pp. 205–208, 2014.

[16] Q. Van den Brande, S. Lemey, J. Vanfleteren, and H. Rogier, "Highly Efficient Impulse-Radio Ultra-Wideband Cavity-Backed Slot Antenna in Stacked Air-Filled Substrate Integrated Waveguide Technology," *IEEE Trans. Antennas Propag.*, vol. 66, no. 5, pp. 2199–2209, May 2018.

[17] K. Y. Kapusuz, S. Lemey, and H. Rogier, "Dual-Polarized 28-GHz Air-Filled SIW Phased Antenna Array for Next-Generation Cellular Systems," in *2019 IEEE International Symposium on Phased Array System Technology (PAST)*, 2019, pp. 1–6.

[18] A. Belenguer, H. Esteban, and V. E. Boria, "Novel Empty Substrate Integrated Waveguide for High-Performance Microwave Integrated Circuits," *IEEE Trans. Microw. Theory Techn.*, vol. 62, no. 4, pp. 832–839, Apr. 2014.

[19] F. Parment, A. Ghiotto, T. Vuong, J. Duchamp, and K. Wu, "Air-Filled Substrate Integrated Waveguide for Low-Loss and High Power-Handling Millimeter-Wave Substrate Integrated Circuits," *IEEE Trans. Microw. Theory Techn.*, vol. 63, no. 4, pp. 1228–1238, 2015.

[20] ——, "Double Dielectric Slab-Loaded Air-Filled SIW Phase Shifters for High-Performance Millimeter-Wave Integration," *IEEE Trans. Microw. Theory Techn.*, vol. 64, no. 9, pp. 2833–2842, 2016.

[21] F. Parment, A. Ghiotto, T.-P. Vuong, J.-M. Duchamp, and K. Wu, "Ka-Band Compact and High-Performance Bandpass Filter Based on Multilayer Air-Filled SIW," *Electron. Lett.*, vol. 53, no. 7, pp. 486–488, 2017.

[22] J. V. Morro, A. Rodríguez, A. Belenguer, H. Esteban, and V. Boria, "Multilevel Transition in Empty Substrate Integrated Waveguide," *Electron. Lett.*, vol. 52, no. 18, pp. 1543–1544, 2016.

[23] Q. Van den Brande, S. Lemey, S. Cuyvers, S. Poelman, L. De Brabander, O. Caytan, L. Bogaert, I. Lima de Paula, S. Verstuyft, A. C. F. Reniers, B. Smolders, B. Kuyken, D. Vande Ginste, and H. Rogier, "A Hybrid Integration Strategy for Compact, Broadband and Highly Efficient Millimeter-Wave On-Chip Antennas," *IEEE Antennas Wireless Propag. Lett.*, pp. 1–1, 2019.

[24] Y. Li and K. Luk, "Low-Cost High-Gain and Broadband Substrate-Integrated-Waveguide-Fed Patch Antenna Array for 60-GHz Band," *IEEE Trans. Antennas Propag.*, vol. 62, no. 11, pp. 5531–5538, 2014.

[25] Y. Li and K.-M. Luk, "60-GHz Substrate Integrated Waveguide Fed Cavity-Backed Aperture-Coupled Microstrip Patch Antenna Arrays," *IEEE Trans. Antennas Propag.*, vol. 63, no. 3, pp. 1075–1085, 2015.

[26] F. Parment, A. Ghiotto, T.-P. Vuong, J.-M. Duchamp, and K. Wu, "Millimetre-Wave Air-Filled Substrate Integrated Waveguide Slot Array Antenna," *Electron. Lett.*, vol. 53, no. 11, pp. 704–706, May 2017.

[27] Z. Qi, X. Li, J. Xiao, and H. Zhu, "Low-Cost Empty Substrate Integrated Waveguide Slot Arrays for Millimeter-Wave Applications," *IEEE Antennas Wireless Propag. Lett.*, vol. 18, no. 5, pp. 1021–1025, 2019.

[28] R. Johnson, *Antenna Engineering Handbook*. New York: McGraw-Hill, 1993.

[29] Y. Lim, Y. J. Cho, T. Oh, Y. Lee, and C. Chae, "Relationship Between Cross-Polarization Discrimination (XPD) and Spatial Correlation in Indoor Small-Cell MIMO Systems," *IEEE Wireless Commun. Lett.*, vol. 7, no. 4, pp. 654–657, 2018.

[30] G. Kumar and K. P. Ray, *Broadband Microstrip Antennas*. Artech house, 2003.

[31] C. Balanis, *Antenna Theory : Analysis and Design*. Hoboken, NJ: Wiley Interscience, 2005.